Journal of Southeast University (English Edition) Vol. 40, No. 2, pp. 210 - 220 June 2024 ISSN 1003—7985

# Mechanical experimental study of a new CFRP grid-bamboo scrimber composite plate

Lü Qingfang[1] Yi Fan[1] Liu Ye[2]

([1]School of Civil Engineering, Southeast University, Nanjing 211189, China)
([2]College of Architecture and Environment, Sichuan University, Chengdu 610065, China)

**Abstract:** A novel composite plate made of carbon fiber-reinforced polymer (CFRP) grids and bamboo scrimber, termed CBCP, was developed to enhance the mechanical properties of bamboo scrimber and reduce its anisotropic defects. To investigate the mechanical behavior of CBCP and assess the influence of its composite fabrication method, uniaxial tensile tests were performed on eight sets of CBCP tensile specimens, and pull-out tests were conducted on eighteen groups of CBCP pull-out specimens. Three similar constitutive models were selected to depict the bond stress-slip curves of the pull-out specimens. The critical anchorage lengths between CFRP grids and bamboo scrimber were determined. The effects of the number of CFRP layers, characteristics of transverse CFRP bundles, and anchorage length on the bonding performance between CFRP grids and bamboo scrimber were analyzed. The results reveal that integrating a CFRP grid can increase the tensile strength of bamboo scrimber, both parallel and perpendicular to the grain, by 35.77% and 135.20%, respectively. This enhancement effectively reduces the anisotropic defects of bamboo scrimber. The increase of the number of grid layers and the grid spacing can enhance the tensile performance of CBCP. With the increase of the anchorage length, the average interface bonding strength decreases exponentially while the peak load slip decreases linearly.

**Key words:** carbon fiber-reinforced polymer; bamboo scrimber; uniaxial tension test; pull-out test; mechanical properties

**DOI:** 10.3969/j.issn.1003-7985.2024.02.012

Bamboo is prominent for its short growth cycle and eco-friendly attributes[1], rendering it a natural green building material. Despite its advantages over common structural timber[2], bamboo faces challenges such as significant variability in mechanical properties and limited corrosion resistance when used as a building material. To address these challenges, researchers have proposed engineering bamboo solutions such as laminated bamboo and bamboo scrimber[3-4]. Studies exploring the mechanical properties of engineered bamboo encompass various aspects[5-6]. Gong et al.[7] demonstrated that bamboo scrimber has significantly higher tensile and compressive strengths compared to timber and other bamboo-based composites. However, as a construction material, bamboo scrimber's load-bearing capacity is relatively low owing to the substantial bidirectional disparities in mechanical properties. Therefore, these challenges highlight the need to enhance bamboo scrimber's strength to advance its application in construction engineering.

Fiber-reinforced polymer (FRP) materials are widely used in construction and bridge engineering, particularly for reinforcing existing structures, owing to their lightweight, high strength, easy processing, and excellent corrosion resistance[8-9]. While most studies have focused on applying FRP in reinforcing concrete structures[10-12], research on applying FRP to bamboo structures is sparse. Shen et al.[13] proposed a modified calculation method based on elastic theory for ultimate deformation in carbon FRP (CFRP) composite bamboo scrimber beams, which was validated through experimental testing. Wei et al.[14] conducted four-point bending tests to assess the flexural performance of FRP-strengthened bamboo scrimber beams. The predominant method of applying FRP materials in engineering involves attaching them to the external surfaces of structures[15]. While this method is straightforward in terms of construction, it faces challenges with interface durability owing to environmental factors, posing debonding risks[16]. To address these issues, near-surface mounted FRP reinforcement has been developed, offering enhanced protection against external environmental damage and improved bonding performance[17].

Ref. [18] investigated the flexural performance of a CFRP grid composite cross-laminated bamboo (CLB) one-way slab. In the resulting one-way slab, the inclusion of CFRP significantly enhanced its mechanical performance and led to distinct failure modes. This study aims to elucidate the mechanical properties of the carbon fiber-reinforced polymer grids-bamboo scrimber compos-

**Received** 2023-01-03, **Revised** 2023-04-20.

**Biography:** Lü Qingfang (1972—), female, doctor, professor, 101011003@seu.edu.cn.

**Foundation items:** The National Natural Science Foundation of China (No. 52378222), Sichuan Science and Technology Program (No. 2023YFS0393).

**Citation:** Lü Qingfang, Yi Fan, Liu Ye. Mechanical experimental study of a new CFRP grid-bamboo scrimber composite plate[J]. Journal of Southeast University (English Edition), 2024, 40(2): 210 - 220. DOI: 10.3969/j.issn.1003-7985.2024.02.012.

ite plate, termed CBCP, and analyze the bonding performance between CFRP grids and bamboo scrimber. In this study, we conducted a series of uniaxial tension tests and pull-out tests on CBCP. Through experiments and parametric analysis, the tensile properties and bonding characteristics of CBCP were systematically explored. The influence of different types of CFRP grids on the mechanical properties of CBCP was discussed to establish a foundational data set for CBCP application.

## 1 Mechanical Tests

### 1.1 Materials

#### 1.1.1 Bamboo scrimber

The bamboo scrimber utilized in this study was derived from moso bamboo aged between 3 and 5 a, featuring a density of 1 236.12 kg/m$^3$ and a moisture content of 8.27%. For the purposes of this study, bamboo scrimber was assumed to possess identical strengths and moduli in two transverse directions that are perpendicular to the grain[19]. The mechanical properties of bamboo scrimber were evaluated according to Chinese standards LY/T 3194—2020[20] and GB/T 40247—2021[21]. The material properties of bamboo scrimber are summarized in Table 1.

**Table 1** Material results of the bamboo scrimber

| Type | Strength/MPa | | Elastic modulus/MPa | |
|---|---|---|---|---|
| | Parallel to grain | Perpendicular to grain | Parallel to grain | Perpendicular to grain |
| Tension | 125.31 | 13.28 | 11 140.07 | 3 783.44 |
| Compression | 113.94 | 50.93 | 19 666.06 | 2 852.03 |
| Bending | 142.95 | 15.60 | 15 543.98 | 1 671.40 |
| Shear | 13.30 | 56.96 | 1 691.72 | 2 935.38 |

#### 1.1.2 CFRP grids

The CFRP grids comprised multiple layers of transverse and longitudinal CFRP bundles, utilizing four types of CFRP bars fabricated with two, three, or four layers of CFRP bundles. Tensile tests on the CFRP bars with a varying number of CFRP bundle layers were conducted in accordance with standards ACI 440.3R-04[22] and GB/T 1447—2005[23]. Table 2 presents the results of the coupon tests.

**Table 2** Tensile strength and elastic modulus of the single CFRP bar

| Layer number of CFRP bundles | Tensile strength/MPa | Elastic modulus/MPa |
|---|---|---|
| 2 | 1 380.73 | 21 782.77 |
| 3 | 974.72 | 23 682.66 |
| 4 | 808.72 | 24 570.26 |

#### 1.1.3 Specimen preparation

The production process of CBCP involved splitting, dipping, hot pressing, and cutting. Initially, raw bamboo was split and processed into bundles of bamboo filaments through crushing and drying. These bundles were then dipped in adhesives, dried, and subsequently hot-pressed at pressures ranging from 16.0 to 17.0 MPa at a temperature of 135.0 ℃. The resulting plate was cured for 1-2 weeks at room temperature before being cut into the desired shapes for testing.

### 1.2 Uniaxial tension tests

Uniaxial tension tests were conducted using a hydraulic servo universal testing machine (MTS 810) at a loading rate of 2 mm/min, as depicted in Fig. 1. The detail information of the specimens for CBCP uniaxial tension is presented in Table 3. Specimens were designated as UTP and UTA for those parallel and perpendicularly to the grain, respectively. The numbers indicate grid spacing, while L1 and L2 represent CFRP grids with 5 and 7 bundle layers.

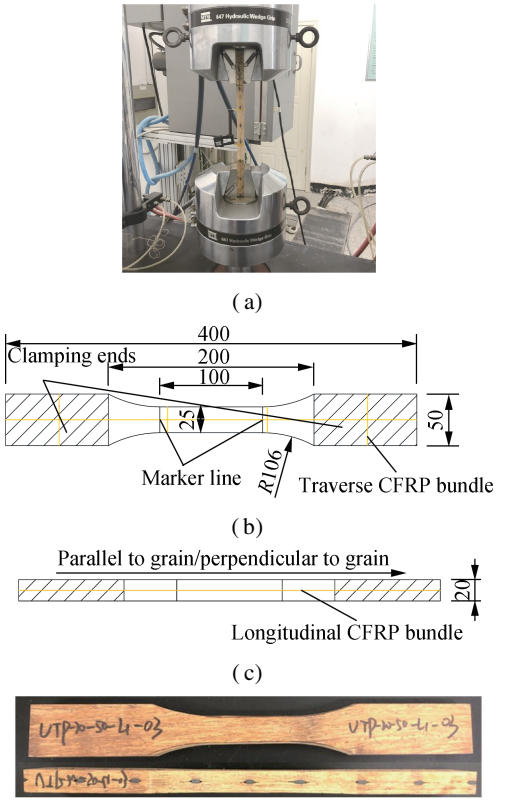


**Fig. 1** Uniaxial tension of the CBCP (unit: mm). (a) Test setup; (b) Front view of the specimen; (c) Side view of the specimen; (d) Front and side photos of the specimen

### 1.3 Pull-out tests

The pull-out specimen involved two bamboo scrimber plates and CFRP grids, as illustrated in Fig. 2. The length of the left bamboo scrimber was designed to prevent any bond slip between CFRP grids and the bamboo scrimber, while the length of the right bamboo scrimber varied to study interfacial behavior.

**Table 3** Detail information of the uniaxial tension of the CBCP

| | Label | Grid spacing/mm | Layer number of CFRP bundles | | Specimen number |
|---|---|---|---|---|---|
| | | | Longitudinal | Transverse | |
| Parallel to grain | UTP-0-0 | | | | 5 |
| | UTP-50-L1 | 50 | 3 | 2 | 5 |
| | UTP-50-L2 | 50 | 4 | 3 | 3 |
| | UTP-100-L1 | 100 | 3 | 2 | 5 |
| Perpendicular to grain | UTA-0-0 | | | | 4 |
| | UTA-50-L1 | 50 | 2 | 3 | 6 |
| | UTA-50-L2 | 50 | 3 | 4 | 4 |
| | UTA-100-L1 | 100 | 2 | 3 | 4 |

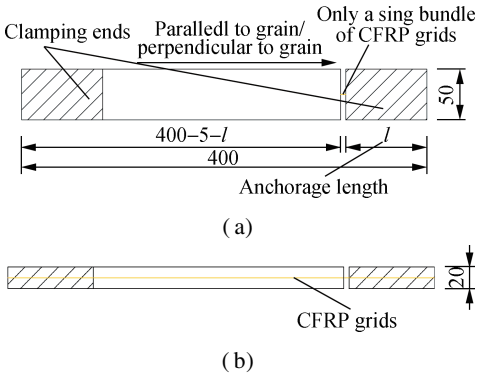


**Fig. 2** Pull-out specimen (unit: mm). (a) Front view; (b) Side view

The pull-out tests were conducted using MTS 810 at 10 mm/min (see Fig. 3). Eighteen groups of pull-out specimens were tested, detailed in Table 4. Pull-out specimen designations are as follows: POP and POA denote pull-out tests parallel and perpendicular to the grain, respectively, with subsequent numbers indicating grid spacing. L1 and L2 represent CFRP grid types, while the final number denotes anchorage length.

**Fig. 3** Test setup for the pull-out test

**Table 4** Detail information of the pull-out specimens

| | Label | Number of transverse CFRP bars | Layer number of CFRP bundle | | Specimen number |
|---|---|---|---|---|---|
| | | | Longitudinal | Transverse | |
| Parallel to grain | POP-50-L1-25 | 0 | 3 | 2 | 2 |
| | POP-50-L1-40 | 1 | 3 | 2 | 2 |
| | POP-50-L1-55 | 2 | 3 | 2 | 5 |
| | POP-50-L1-70 | 1 | 3 | 2 | 1 |
| | | 2 | 3 | 2 | 2 |
| | POP-50-L1-85 | 2 | 3 | 2 | 4 |
| | POP-50-L1-100 | 2 | 3 | 2 | 5 |
| | POP-50-L1-115 | 2 | 3 | 2 | 4 |
| | POP-50-L2-70 | 2 | 4 | 3 | 4 |
| | POP-100-L1-70 | 1 | 3 | 2 | 3 |
| Perpendicular to grain | POA-50-L1-25 | 0 | 2 | 3 | 2 |
| | POA-50-L1-40 | 0 | 2 | 3 | 3 |
| | POA-50-L1-55 | 1 | 2 | 3 | 5 |
| | POA-50-L1-70 | 1 | 2 | 3 | 1 |
| | | 2 | 2 | 3 | 5 |
| | POA-50-L1-85 | 2 | 2 | 3 | 5 |
| | POA-50-L1-100 | 2 | 2 | 3 | 4 |
| | POA-50-L1-115 | 2 | 2 | 3 | 4 |
| | POA-50-L2-70 | 2 | 3 | 4 | 3 |
| | POA-100-L1-70 | 1 | 2 | 3 | 3 |

## 2 Test Results and Experimental Observations

### 2.1 Tensile behavior of CBCP

#### 2.1.1 Failure modes under uniaxial tension

Fig. 4 illustrates the failure surfaces of uniaxial tension specimens. Two distinct failure modes were observed in bamboo scrimber specimens without CFRP grids: fracture of bamboo fibers (F) and separation of bamboo fibers (S). Conversely, CBCP specimens exhibited three failure modes: failure of bamboo scrimber parallel to the grain

and CFRP grids (FC), failure of bamboo scrimber perpendicular to the grain and CFRP grids (FS), and failure of bamboo scrimber perpendicular to the grain and partial failure of CFRP grids (PA).

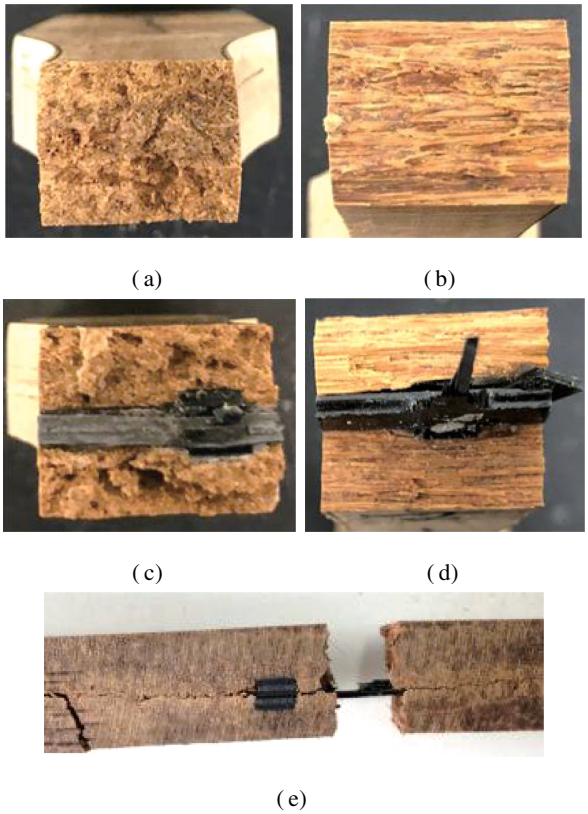


**Fig. 4** Failure modes in uniaxial tension tests. (a) F; (b) S; (c) FC; (d) FS; (e) PA

### 2.1.2 Force-displacement curves

The test results of the uniaxial tension are listed in Table 5. $F_{max}$ is the peak load at the failure point and $f_t$ is the tensile strength calculated as

$$f_t = \frac{F_{max}}{bd} \tag{1}$$

where $b$ and $d$ are the average values of the measured width and thickness, respectively.

The force-displacement curves of CBCP specimens parallel to the grain exhibit three distinct stages, as illustrated in Fig. 5(a), including the linear stage, the nonlinear stage, and the failure stage. During the linear stage, the force increases linearly with displacement until reaching point $C$, followed by a decrease in slope during the nonlinear stage due to bamboo fiber fracture. At point $D$, the force peaks before experiencing a dramatic decrease, indicating brittle failure.

As shown in Fig. 5(b), the force-displacement curves of CBCP specimens perpendicular to the grain also display three stages: linear, plastic, and failure. The linear and failure stages resemble those observed in specimens parallel to the grain. However, the plastic stage, starting

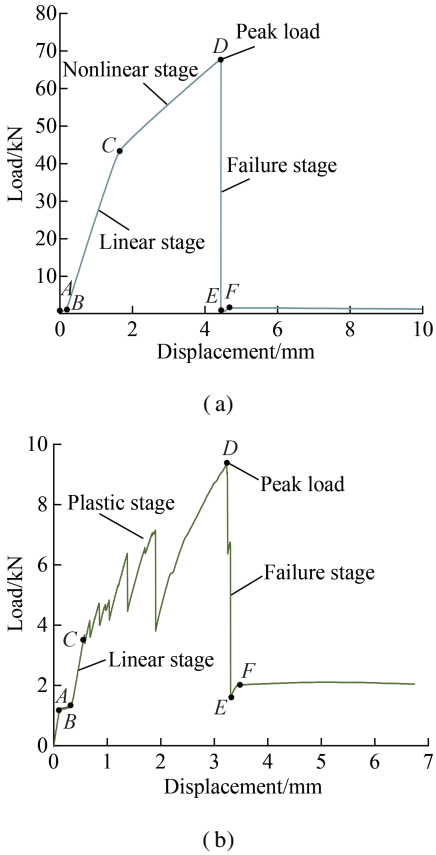


**Fig. 5** Stage definition of the force-displacement curve. (a) Parallel to the grain; (b) Perpendicular to the grain

at point $C$, exhibits significant fluctuations owing to bamboo fiber separation, contrasting with the nonlinear stage in Fig. 5(a). At point $D$, the force peaks at a relatively lower level compared to that in Fig. 5(a).

### 2.1.3 Stress-strain curves

Only the stress-strain curve, derived from extensometer data in the early loading stage, was analyzed. Stress increased linearly with strain until brittle failure occurred in the uniaxial tension test. Fig. 6 displays the stress-strain curves of representative groups of uniaxial tension specimens. The average modulus of elasticity for each specimen group is depicted in Table 5.

## 2.2 Interfacial behavior of CBCP

### 2.2.1 Failure modes under pull-out

The pull-out test yielded two types of failure modes: bond failure (BF) and tensile failure (TF), as illustrated in Fig. 7. In specimens experiencing BF, the force increased linearly with displacement until the peak point without any relative slip between the CFRP grids and the bamboo scrimber. Subsequently, interfacial debonding occurred, resulting in a sudden decrease in force, while residual force (approximately 50%-60% of the peak load) persisted owing to interfacial friction until the total pull-out of CFRP grids (see Figs. 7 and 8(a)). After debonding, no damage was observed on the

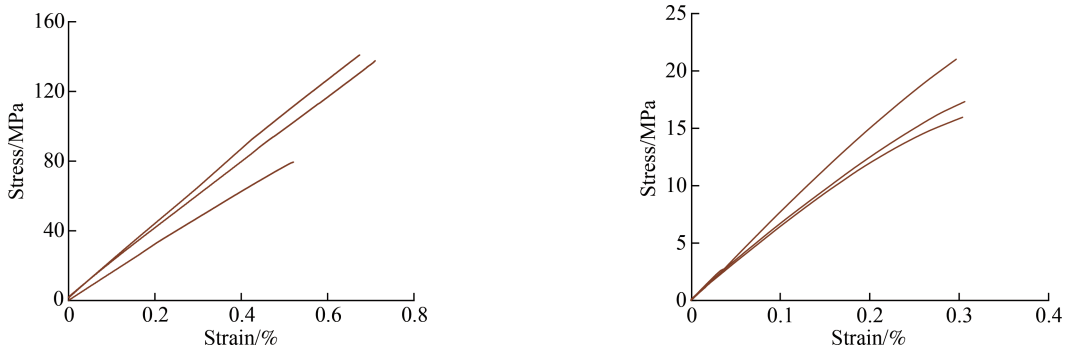


**Fig. 6** Stress-strain curves. (a) UTP-100-L1; (b) UTA-100-L1

**Table 5** Test results of uniaxial tension tests

| Label | $F_{max}$/kN | Tensile strength $f_t$/MPa | Peak displacement/mm | Failure mode | Average modulus of elasticity/GPa |
|---|---|---|---|---|---|
| UTP-0-0 | 56.188 4 | 108.9 | 5.7 | F | 12.04 |
| UTP-50-L1 | 59.908 0 | 128.6 | 5.9 | FC | 16.93 |
| UTP-50-L2 | 71.306 0 | 147.9 | 5.1 | FC | 17.98 |
| UTP-100-L1 | 71.623 0 | 146.9 | 5.0 | FC | 18.85 |
| UTA-0-0 | 5.871 4 | 11.6 | 1.0 | S | 3.49 |
| UTA-50-L1 | 7.710 1 | 15.5 | 1.8 | FS | 5.84 |
| UTA-50-L2 | 12.298 0 | 25.3 | 1.9 | PA | 7.12 |
| UTA-100-L1 | 10.444 8 | 21.5 | 1.5 | PA | 6.16 |

(a) (b)

**Fig. 7** Failure modes in the pull-out test. (a) Bond failure; (b) Tensile failure

CFRP grids, although some bamboo scrimber residue remained. Notably, BF occurred only when the bonding length was smaller than the critical anchorage length.

In specimens experiencing TF, the combined effect of chemical bonding and mechanical interlocking provided interfacial shear resistance that exceeded the tensile strength of the composite specimen. Similar to BF, the force-displacement behavior remained linear until reaching the peak. Beyond this point, the longitudinal bars in the CFRP grids gradually fractured, causing force fluctuations within a small displacement range. At approximately 5 mm of displacement, most carbon fibers had fractured, and the force decreased to about 2 kN. Further displacement deactivated carbon fibers, causing the force to reduce to zero (see Fig. 8(b)).

### 2.2.2 Constitutive model of the bond stress-slip behavior

The results of the pull-out test are summarized in Tables 6 and 7. $F_{max}$ represents the peak load at the failure point, and $\tau_m$ denotes the average interfacial bonding strength between the longitudinal grid and the bamboo scrimber, calculated as

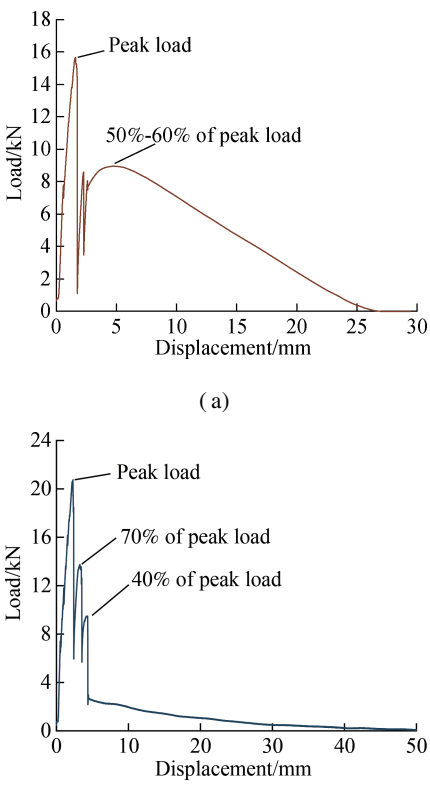


**Fig. 8** Force-displacement curves of pull-out specimens for different failure modes. (a) Bond failure; (b) Tensile failure

$$\tau_m = \frac{F_{max}}{2(w+t)l} \quad (2)$$

where $w$, $t$ and $l$ are the average values of the measured width, thickness and anchorage length of longitudinal grids, respectively.

**Table 6** Test results of the pull-out test parallel to the grain

| Label | $n$ | $l$/mm | $w$/mm | $t$/mm | $F_{max}$/N | $\tau_m$/MPa | Peak load slip/mm | Failure mode |
|---|---|---|---|---|---|---|---|---|
| POP-50-L1-25 | 0 | 25 | 7.17 | 5.46 | 15 651.42 | 24.81 | 1.264 | BF |
| POP-50-L1-40 | 1 | 40 | 6.94 | 5.47 | 18 470.99 | 18.61 | 1.234 | BF |
| POP-50-L1-55 | 1 | 55 | 7.91 | 5.40 | 17 034.20 | 11.63 | 1.095 | BF |
| | 2 | 55 | 7.25 | 5.65 | 19 540.52 | 13.73 | 0.994 | TF |
| POP-50-L1-70 | 1 | 70 | 7.27 | 5.46 | 15 863.25 | 8.90 | 1.553 | TF |
| | 2 | 70 | 6.97 | 5.34 | 17 384.36 | 10.10 | 0.423 | TF |
| POP-50-L1-85 | 2 | 85 | 7.33 | 5.44 | 16 559.22 | 7.64 | 0.867 | TF |
| POP-50-L1-100 | 2 | 100 | 7.38 | 5.57 | 19 446.24 | 7.52 | 0.410 | TF |
| POP-50-L1-115 | 2 | 115 | 7.32 | 5.51 | 20 015.91 | 6.78 | 0.177 | TF |
| POP-50-L2-70 | 2 | 70 | 7.48 | 7.49 | 21 248.97 | 10.15 | 0.900 | TF |
| POP-100-L1-70 | 1 | 70 | 7.10 | 5.41 | 15 782.35 | 9.01 | 0.498 | TF |

Note: $n$ denotes the number of transverse CFRP bars in the anchorage section.

**Table 7** Test results of the pull-out test perpendicular to the grain

| Label | $n$ | $l$/mm | $w$/mm | $t$/mm | $F_{max}$/N | $\tau_m$/MPa | Peak load slip/mm | Failure mode |
|---|---|---|---|---|---|---|---|---|
| POA-50-L1-25 | 0 | 25 | 7.92 | 2.90 | 9 716.08 | 18.03 | 1.057 | TF |
| POA-50-L1-40 | 0 | 40 | 7.74 | 2.85 | 1 2678.46 | 14.96 | 1.176 | TF |
| POA-50-L1-55 | 1 | 55 | 7.47 | 3.34 | 9 521.25 | 8.02 | 1.127 | TF |
| POA-50-L1-70 | 1 | 70 | 7.46 | 3.26 | 5 283.44 | 3.52 | 1.226 | TF |
| | 2 | 70 | 8.00 | 3.49 | 11 645.61 | 7.24 | 1.330 | TF |
| POA-50-L1-85 | 2 | 85 | 7.48 | 3.66 | 10 323.10 | 5.45 | 0.521 | TF |
| POA-50-L1-100 | 2 | 100 | 7.40 | 3.38 | 11 636.68 | 5.40 | 0.065 | TF |
| POA-50-L1-115 | 2 | 115 | 7.75 | 3.23 | 10 166.99 | 4.02 | 0.750 | TF |
| POA-50-L2-70 | 2 | 70 | 8.10 | 4.61 | 11 690.63 | 6.57 | 0.573 | TF |
| POA-100-L1-70 | 1 | 70 | 7.22 | 3.30 | 5 079.60 | 3.45 | 0.239 | TF |

Bond stress-slip curves of representative specimens were fitted using the MBPE model[24], CMR model[24], and smooth curve model[25]. The fitting results are presented in Fig. 9. The values of the coefficient of determination ($R^2$) of the fitting results are presented in Table 8.

The bond stress-slip curves of pull-out composite specimen groups revealed three stages: ascent, descent, and residual. According to the fitting results, the MBPE model exhibited satisfactory performance solely in the ascent stage for the parallel-to-grain specimens and both the ascent and descent stages for the perpendicular-to-grain specimens. However, the residual stage of the MBPE model was not suitable for the bond stress-slip curves of the CFRP grid and bamboo scrimber. Conversely, the CMR model effectively fitted the ascent stage of the bond stress-slip curves for all specimen groups, as evidenced by the high $R^2$ values. Lastly, the smooth curve model was applicable only to the descent stage of the bond stress-slip curve for the perpendicular-to-grain specimens.

### 2.2.3 Critical anchorage length

From Table 6, composite specimens featuring 3 layers of longitudinal CFRP bars exhibited BF at a 40 mm anchorage length, while specimens demonstrated both BF and TF at a 55 mm anchorage length. Therefore, an anchorage length of 55 mm was identified as the critical anchorage length for CBCP pull-out specimens parallel to the grain with 3 layers of CFRP grids.

The calculation method for anchorage length follows GB 50010—2010[26]. Fig. 10 shows the calculation model for the critical anchoring length, which can be calculated according to the equilibrium of force as

$$l_a = k\frac{wt}{2(w+t)}\frac{f_c}{f_b} \quad (3)$$

where $l_a$ is the critical anchorage length of CFRP grids; $w$ and $t$ are the width and thickness of longitudinal CFRP bar, respectively; $f_c$ is the tensile strength of CFRP grids; $f_b$ is the tensile strength of the bamboo scrimber.

By substituting the data obtained from the pull-out test into Eq. (3), we can derive the calculation formula of the critical anchorage length for CBCP pull-out specimens parallel to the grain with 3 layers of longitudinal CFRP bars as

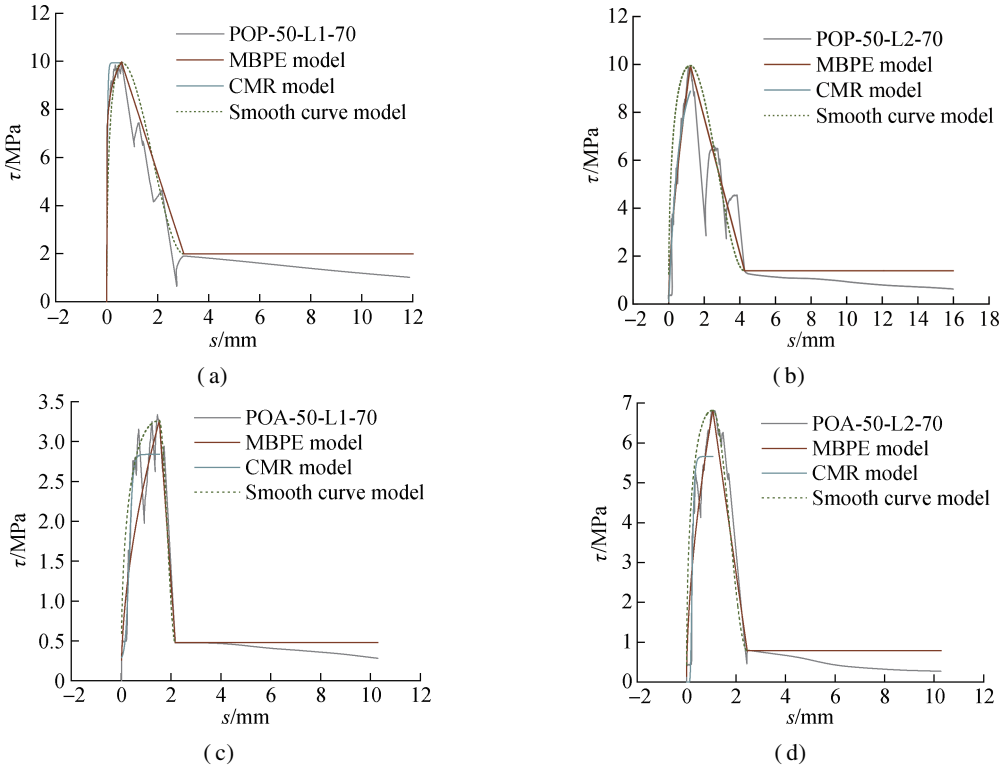


**Fig. 9** Fitting results of test results and theoretical models of bond stress-slip curves. (a) POP-50-L1-70; (b) POP-50-L2-70; (c) POA-50-L1-70; (d) POA-50-L2-70

**Table 8** $R^2$ of fitting results

| Label | MBPE model | | | CMR model | Smooth curve model | |
|---|---|---|---|---|---|---|
| | Ascent stage | Descent stage | Residual stage | Ascent stage | Ascent stage | Descent stage |
| POP-50-L1-70 | 0.89 | 0.77 | −4.08 | 0.82 | −0.42 | 0.74 |
| POP-50-L2-70 | 0.93 | 0.01 | −2.09 | 0.95 | 0.08 | −0.71 |
| POA-50-L1-70 | 0.76 | 0.88 | −1.63 | 0.92 | 0.55 | 0.94 |
| POA-50-L2-70 | 0.83 | 0.9 | −3.55 | 0.89 | 0.20 | 0.96 |

$$l_a = 2.26 \frac{wt}{w+t} \frac{f_c}{f_b} \tag{4}$$

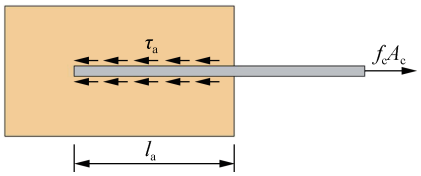


**Fig. 10** Calculation method of critical anchoring length

Owing to the limited number of tests conducted in the pull-out test of specimens perpendicular to the grain (see Table 7), it was not feasible to determine the critical anchorage length of CBCP pull-out specimens.

## 3 Discussion

### 3.1 Parametric analysis of uniaxial tension of CBCP

In the uniaxial tensile tests of CBCP, specimen groups UTP-0-0 and UTA-0-0 serve as the control group. The variations in tensile strength, elastic modulus, and peak displacement compared to the control groups for each specimen group are presented in Table 9.

**Table 9** Average parameters of each specimen group

| Label | Tensile strength | | Elastic modulus | | Peak displacement | |
|---|---|---|---|---|---|---|
| | $f_t$/MPa | Variation/% | $E$/GPa | Variation/% | $s_p$/mm | Variation/% |
| UTP-0-0 | 108.90 | | 12.04 | | 5.73 | |
| UTP-50-L1 | 128.59 | 18.08 | 16.93 | 40.61 | 5.89 | 2.79 |
| UTP-50-L2 | 147.85 | 35.77 | 17.81 | 47.92 | 5.14 | −10.30 |
| UTP-100-L1 | 146.90 | 34.89 | 18.85 | 56.56 | 5.01 | −12.57 |
| UTA-0-0 | 11.56 | | 3.49 | | 0.98 | |
| UTA-50-L1 | 17.52 | 51.56 | 5.84 | 67.33 | 2.14 | 118.37 |
| UTA-50-L2 | 29.27 | 153.20 | 7.12 | 104.01 | 2.09 | 113.27 |
| UTA-100-L1 | 21.53 | 86.25 | 6.16 | 76.50 | 1.47 | 50.00 |

Note: $s_p$ denotes the peak displacements in uniaxial tensile tests.

#### 3.1.1 Effect of the CFRP grids

Table 9 demonstrates that integrating CFRP grids significantly enhances the tensile strength and elastic modulus of bamboo scrimber and has a more significant effect on the perpendicular-to-grain direction of bamboo scrimber (maximum increase of 35.77% for specimens parallel to the grain and 153.20% for specimens perpendicular to the grain), effectively mitigating its inherent two-way anisotropic defects.

#### 3.1.2 Effect of the layer number of CFRP grids

Comparing groups UTP-50-L1 and UTP-50-L2, along with UTA-50-L1 and UTA-50-L2, reveals that increasing the number of longitudinal CFRP grids enhances the tensile strength and elastic modulus of CBCP, especially perpendicularly to the grain. Material data presented in Section 1.1 indicate that CFRP grids possess substantially higher tensile strength and elastic modulus compared to those of the bamboo scrimber. Consequently, as the layer number of CFRP grids increases, the ratio of CFRP to bamboo fibers' cross-sectional area ratio rises, boosting CBCP's tensile properties.

#### 3.1.3 Effect of grid spacing

Comparing specimen groups with different grid spacings (UTP-50-L1 and UTP-100-L1, UTA-50-L1 and UTA-100-L1) reveals that increasing the spacing between transverse CFRP bundles enhances tensile strength and elastic modulus but reduces peak displacement. This is attributed to the reduced gaps on the surface of the CFRP grids (see Fig. 11), improving the synergy between the bamboo scrimber and CFRP grids, thereby enhancing the tensile properties of the composite specimens. However, given the inherent variability in bamboo scrimber specimens, further experimental verification is needed to determine the impact on peak displacement.

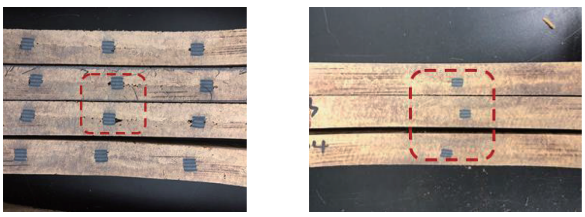

(a) (b)

**Fig. 11** Voids on the surface of CFRP grids. (a) Grid spacing of 50 mm; (b) Grid spacing of 100 mm

### 3.2 Parametric analysis of interfacial bonding of CBCP

#### 3.2.1 Effect of the layer number of CFRP grids

Analysis of the test results presented in Tables 6 and 7 reveals that, compared to POP-50-L1-70, the average interface bond strength of POP-50-L2-70 increased by 4.54%, and the peak load slip increased by 12.5%. On the other hand, when compared to POA-50-L1-70, the average interface bond strength of POA-50-L2-70 decreased by 9.25%, and the peak load slip decreased by 56.91%. The peak bond stress of the pull-out tests parallel to the grain was found to increase with an additional layer of longitudinal CFRP bundles. Conversely, in pull-out tests conducted perpendicularly to the grain, peak bond stress notably decreases with more CFRP grid layers. This decline in bonding performance can be attributed to the increased cross-sectional area ratio between the CFRP and bamboo scrimber, resulting in a higher number of voids between the CFRP grid surfaces perpendicular to the grain, which consequently reduces their bonding performance with bamboo scrimber.

#### 3.2.2 Effect of the transverse CFRP bundles

For both the parallel and perpendicular orientations relative to the grain, we compared the test results of specimens in groups POP-50-L1-70 and POA-50-L1-70, which feature 1 and 2 transverse bundles in the anchorage section, respectively. When the anchorage length is consistent, an increase in the number of transverse bundles in the anchorage section causes the average interface bond strength to rise, resulting in a 15.30% increase for specimens parallel to the grain and a 105.68% increase for specimens perpendicular to the grain. This phenomenon is attributed to the robust integration of transverse CFRP bundles and longitudinal CFRP bundles at the nodes using epoxy resin, thereby requiring the pull-out test to surpass both the bond strength of the epoxy resin and the constraint of the transverse bundles.

When comparing the average interface bond strength and peak load slip across specimen groups with different transverse grid spacings (POP-50-L1-70 and POP-100-L1-70, POA-50-L1-70 and POA-100-L1-70), with the same anchorage length and number of transverse bundles in the anchorage section, increasing the spacing of transverse bundles from 50 to 100 mm reduces the peak load slip for specimens oriented both parallel and perpendicular to the grain, while the average interfacial bond strength changes minimally.

#### 3.2.3 Effect of the anchorage length

Fig. 12 illustrates the bond stress-slip curves for each anchorage length group, revealing a gradual decrease in peak load and a leftward shift in the curve as the anchorage length increases. The average interfacial bond strength and peak load slip data at various anchorage lengths were subjected to a fitting analysis, as depicted in Figs. 13 and 14.

With the increase in the anchorage length, both the peak load slip and the average interface bond strength exhibit a decreasing trend. This occurs because as the anchorage length increases, the bond strength increases, resulting in a corresponding decrease in slip displacement at the peak load. Additionally, as the anchorage length increases, the contact area of the interface also expands, leading to a decrease in the average interface bond stress.

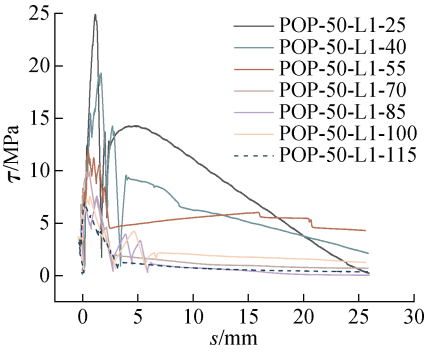


(a)

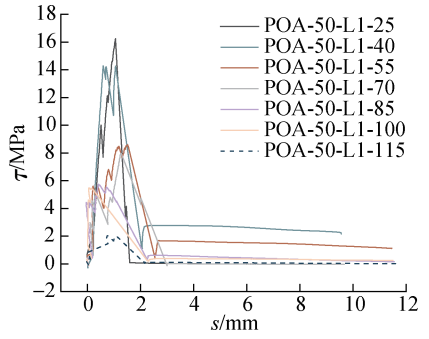


(b)

**Fig. 12** Bond stress-slip curves for different anchorage lengths. (a) Parallel to the grain; (b) Perpendicular to the grain

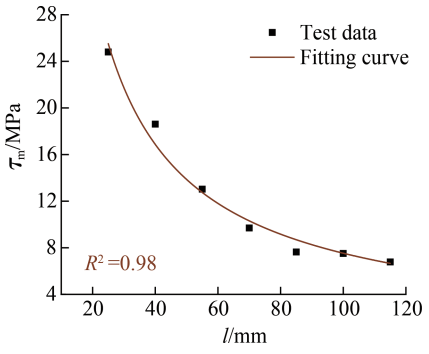


(a)

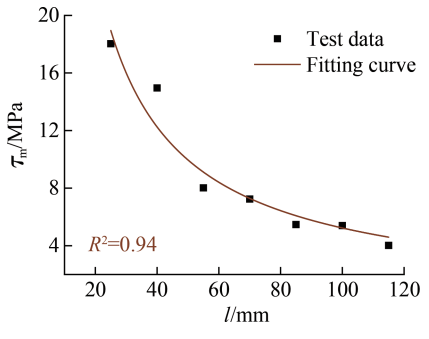


(b)

**Fig. 13** Fitting results of anchorage length and average interfacial bond strength. (a) Parallel to the grain; (b) Perpendicular to the grain

The fitting results show that as the anchorage length increases, the average interface bond strength decreases

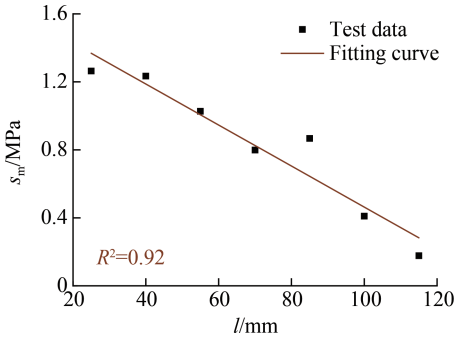


(a)

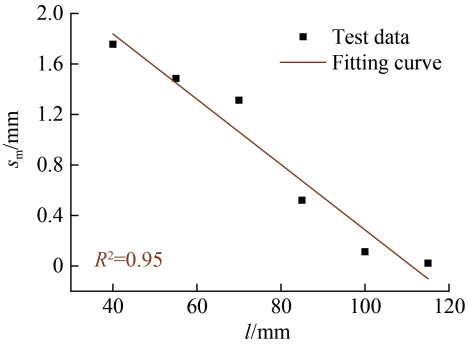


(b)

**Fig. 14** Fitting results of anchorage length and peak load slip displacement. (a) Parallel to the grain; (b) Perpendicular to the grain

according to a power function, while the peak load slip decreases linearly. The relationship for the specimens parallel to the grain can be expressed as

$$\tau_m = 433.57 l^{-0.88} \tag{5}$$

$$s_m = -0.012 l + 1.670 \tag{6}$$

where $\tau_m$ is the average interfacial bond strength; $s_m$ is the slip displacement corresponding to the peak load.

The relationship for the specimens perpendicular to grain can be expressed as

$$\tau_m = 375.98 l^{-0.928} \tag{7}$$

$$s_m = -0.025\ 9 l + 2.877\ 3 \tag{8}$$

## 4 Conclusions

1) In the uniaxial tension tests of CBCP, three failure modes were identified. The tensile stress-strain relationship of CBCP tensile specimens is linear, and their damage mode occurs through brittle failure.

2) Incorporating CFRP grids into bamboo scrimber significantly enhances its tensile strength and elastic modulus, effectively mitigating the inherent two-way variability of the original material. The tensile properties of CBCP specimens improve with additional layers of CFRP grids.

3) The pull-out tests revealed two failure modes. Based on these results, a formula was developed to calculate the critical anchorage length of CBCP featuring 3 layers of longitudinal CFRP bundles in the parallel-to-grain direction.

4) The bond stress-slip curves are characterized by three stages: ascent, descent, and residual. To analyze these curves, three constitutive models were applied to fit the test data, revealing partial degrees of applicability to the bond stress-slip curves of CFRP grids and bamboo scrimber.

5) Increasing the number of CFRP grid layers enhances the bond strength of CFRP parallel to the grain. However, it significantly weakens the bond strength of CFRP perpendicular to the grain. Augmenting the number of transverse CFRP bundles in the anchorage section enhances bonding performance, especially in the perpendicular direction to the grain. Widening the grid spacing reduces the peak load slip between CFRP grids and bamboo scrimber without notably affecting the average interfacial bond strength.

6) As the anchorage length increases, both peak load slip and average interface bond strength decrease. The reduction in the average interface bond strength can be described by a power function, while the peak load slip decreases linearly.

## References


[1] Xiao Y, Yang R Z, Shan B. Production, environmental impact and mechanical properties of glubam[J]. *Construction and Building Materials*, 2013, **44**: 765 − 773. DOI: 10.1016/j.conbuildmat.2013.03.087.

[2] Chung K F, Yu W K. Mechanical properties of structural bamboo for bamboo scaffoldings[J]. *Engineering Structures*, 2002, **24**(4): 429 − 442. DOI: 10.1016/s0141-0296(01)00110-9.

[3] Mahdavi M, Clouston P L, Arwade S R. Development of laminated bamboo lumber: Review of processing, performance, and economical considerations[J]. *Journal of Materials in Civil Engineering*, 2011, **23**(7): 1036 − 1042. DOI: 10.1061/(asce)mt.1943-5533.0000253.

[4] Sharma B, Gatóo A, Bock M, et al. Engineered bamboo for structural applications[J]. *Construction and Building Materials*, 2015, **81**: 66 − 73. DOI: 10.1016/j.conbuildmat.2015.01.077.

[5] Lee C H, Chung M J, Lin C H, et al. Effects of layered structure on the physical and mechanical properties of laminated moso bamboo (Phyllosachys edulis) flooring[J]. *Construction and Building Materials*, 2012, **28**(1): 31 − 35. DOI: 10.1016/j.conbuildmat.2011.08.038.

[6] Lü Q F, Wang W Y, Liu Y. Experimental study on mechanical properties of cross-laminated bamboo slabs after one-sided fire[J]. *Journal of Southeast University* (*Natural Science Edition*), 2021, **51**(2): 212 − 218. DOI: 10.3969/j.issn.1001-0505.2021.02.004. (in Chinese)

[7] Gong Y C, Zhang C Q, Zhao R J, et al. Experimental study on tensile and compressive strength of bamboo scrimber[J]. *Bioresources*, 2016, **11**(3): 7334 − 7344. DOI: 10.15376/biores.11.3.7334-7344.

[8] Gu D S, Wu G, Wu Z S. Ultimate flexural strength of normal section of FRP-confined RC circular columns[J]. *Journal of Southeast University* (*English Edition*), 2010, **26**(1): 107 − 111. DOI: 10.3969/j.issn.1003-7985.2010.01.022.

[9] Shi J W, Wu Q Q, Wu S X, et al. Analysis on disease repair effects of hollow slab bridge strengthened with prestressed FRP grid[J]. *Journal of Southeast University* (*Natural Science Edition*), 2024, **54**(2): 407 − 415. DOI: 10.3969/j.issn.1001-0505.2024.02.018. (in Chinese)

[10] Fang H, Xu X, Liu W Q, et al. Flexural behavior of composite concrete slabs reinforced by FRP grid facesheets[J]. *Composites Part B*: *Engineering*, 2016, **92**: 46 − 62. DOI: 10.1016/j.compositesb.2016.02.029.

[11] Wang T, Fan X Q, Gao C S, et al. Database-based error analysis of calculation methods for shear capacity of FRP-reinforced concrete beams without web reinforcement[J]. *Journal of Southeast University* (*English Edition*), 2023, **39**(3): 301 − 313. DOI: 10.3969/j.issn.1003-7985.2023.03.011.

[12] Fan X C, Huang Y C, Zhang A, et al. Analysis of bonding properties of recycled tire steel fiber reinforced concrete with BFRP bars[J]. *Journal of Southeast University* (*Natural Science Edition*), 2024, **54**(2): 389 − 397. DOI: 10.3969/j.issn.1001-0505.2024.02.016. (in Chinese)

[13] Shen Y R, Huang D S, Zhou A P, et al. An inelastic model for ultimate state analysis of CFRP reinforced PSB beams[J]. *Composites Part B*: *Engineering*, 2017, **115**: 266 − 274. DOI: 10.1016/j.compositesb.2016.09.089.

[14] Wei Y, Ji X W, Duan M J, et al. Flexural performance of bamboo scrimber beams strengthened with fiber-reinforced polymer[J]. *Construction and Building Materials*, 2017, **142**: 66 − 82. DOI: 10.1016/j.conbuildmat.2017.03.054.

[15] Arduini M, Nanni A. Parametric study of beams with externally bonded FRP reinforcement[J]. *ACI Structural Journal*, 1997, **94**(5): 493 − 501.

[16] Shi J W, Xu B L. Bond behavior and capacity prediction of FRP laminate-to-concrete interface under mixed-mode loading[J]. *Journal of Southeast University* (*Natural Science Edition*), 2022, **53**(3): 489 − 496. DOI: 10.3969/j.issn.1001-0505.2022.03.009. (in Chinese)

[17] Chun Q, Zhang Y, Pan J W. Experimental study on bending behaviors of timber beams strengthened with near-surface mounted CFRP sheets[J]. *Journal of Southeast University* (*Natural Science Edition*), 2012, **42**(6): 1146 − 1150. DOI: 10.3969/j.issn.1001-0505.2012.06.023. (in Chinese)

[18] Lü Q F, Wang W Y, Liu Y. Flexural performance of cross-laminated bamboo (CLB) slabs and CFRP grid composite CLB slabs[J]. *Advances in Civil Engineering*, 2019, **2019**: 6980782. DOI: 10.1155/2019/6980782.

[19] Huang D S, Bian Y L, Zhou A P, et al. Experimental study on stress-strain relationships and failure mechanisms of parallel strand bamboo made from phyllostachys[J]. *Construction and Building Materials*, 2015, **77**: 130 − 138. DOI: 10.1016/j.conbuildmat.2014.12.012.

[20] National Forestry and Grassland Administration. Structural bamboo scrimber: LY/T 3194—2020[S]. Beijing: Standards Press of China, 2020. (in Chinese)

[21] National Forestry and Grassland Administration. Bamboo

scrimber: GB/T 40247—2021 [S]. Beijing: Standards Press of China, 2021. (in Chinese)
[22] American Concrete Institute. Guide test methods for fiber-reinforced polymers (FRPs) for reinforcing or strengthening concrete structures: ACI 440.3R-2004[S]. Farmington Hill, MI, USA: American Concrete Institute, 2004
[23] China National Institute of Standardization. Fiber-reinforced plastics composites-determination of tensile properties: GB/T 1447—2005[S]. Beijing: Standards Press of China, 2005. (in Chinese)
[24] Cosenza E, Manfredi G, Realfonzo R. Development length of FRP straight rebars[J]. *Composites Part B*: *Engineering*, 2002, **33**(7): 493 - 504. DOI: 10.1016/S1359-8368(02)00051-3.
[25] Gao D Y, Zhu H T, Xie J J. The constitutive models for bond slip relation between FRP rebars and concrete[J]. *Industrial Construction*, 2003, **33**(7): 41 -43, 82. DOI: 10.13204/j.gyjz2003.07.011. (in Chinese)
[26] Ministry of Housing and Urban-Rural Development of the People's Republic of China. Code for design of concrete structures: GB 50010—2010 [S]. Beijing: Standards Press of China, 2010. (in Chinese)

# 新型 CFRP 网格-重组竹复合板力学试验研究

吕清芳[1] 易 凡[1] 刘 烨[2]

([1]东南大学土木工程学院, 南京 211189)
([2]四川大学建筑与环境学院, 成都 610065)

**摘要**:为提高重组竹的力学性能并减轻其各向异性缺陷,设计了一种新型 CFRP 网格-重组竹复合板(CBCP). 分别对 8 组 CBCP 拉伸试样和 18 组 CBCP 拉拔试样进行单轴拉伸试验和拉拔试验,以分析其力学行为并评估复合方法的影响. 选择 3 个相似的构成模型对拉拔试样的黏结应力-滑移曲线进行拟合,根据试验结果确定 CFRP 网格和重组竹的临界锚固长度及计算方法,并分析讨论了 CFRP 层数、横向 CFRP 束特性和锚固长度对 CFRP 网格与重组竹黏结性能的影响. 结果表明,复合 CFRP 网格可使重组竹的顺纹和横纹抗拉强度分别提高 35.77% 和 135.20%,从而改善了重组竹的各向异性缺陷. 增加网格层数和间距可提高 CBCP 的拉伸性能. 随着锚固长度的增加,平均界面黏结强度呈幂函数递减,而峰值载荷滑移则线性递减.

**关键词**:CFRP;重组竹;单轴拉伸试验;拉拔试验;力学性能
**中图分类号**:TU366.1